v. 3, n. 13, 2023

Journal of
Engineering
Research

BEHAVIOR OF A 2.66%C-17.9%NI GRAY CAST IRON WITH AN AUSTENITIC MATRIX UNDER SIMULATED MARINE CORROSION

Héctor Bruna
Departamento de Ingeniería Metalúrgica,
Universidad de Santiago de Chile
Santiago - Chile
https://orcid.org/0000-0003-0157-3620

Alfredo Artigas
Departamento de Ingeniería Metalúrgica,
Universidad de Santiago de Chile
Santiago - Chile
https://orcid.org/0000-0003-2070-0517

Rodrigo Allende
Departamento de Ingeniería Metalúrgica,
Universidad de Santiago de Chile
Santiago - Chile
https://orcid.org/0000-0002-2115-8160

Alberto Monsalve
Departamento de Ingeniería Metalúrgica,
Universidad de Santiago de Chile
Santiago - Chile
https://orcid.org/0000-0002-5772-8815

Linton Carvajal
Departamento de Ingeniería Metalúrgica,
Universidad de Santiago de Chile
Santiago - Chile
https://orcid.org/0000-0002-5414-2755

Oscar Bustos
Departamento de Ingeniería Metalúrgica,
Universidad de Santiago de Chile
Santiago - Chile
https://orcid.org/0000-0001-7663-1528

Abstract: This article presents the characterization of a gray cast iron with an austenitic matrix subjected to a simulated marine atmosphere. The corrosion process was carried out through the same accelerated corrosion tests which in 40 days evaluate long periods of corrosion (approximately 20 years) in steels. Corrosion products were analyzed by scanning electron microscopy and gravimetric techniques, obtaining curves of corroded thickness over time. The results were compared with previously reported real-time corrosion data for cast austenitic steels and austenitic iron and they show that the corrosion products are consistent with what is reported in the literature, in addition to being comparable with data obtained in a mid-tide marine atmosphere. The experimental results also confirm that the corrosion mechanism is different from that described for steels.
Keywords: Gray cast iron, corrosion, austenite.

INTRODUCTION

Corrosive processes entail a series of problems worldwide (Harsimran et al., 2021) contributing to an increase in maintenance costs and a decrease in the safety of people and the environment. According to a study published by NACE International, the estimated global cost of corrosion is US$2.5 trillion, equivalent to approximately 3.4% of the world's gross domestic product (Schmitt, s. f.).

Dealing with this phenomenon implies extending the service life of the exposed materials, reducing maintenance costs, and avoiding accidents resulting from fractures caused by corrosion (*AMPP,2021)*. Due to its salinity, the marine environment is one of the most corrosive atmospheres, which makes it of great interest for current and future research.

Gray cast irons, or simply gray irons, constitute a family of Fe-C-Si alloys associated

with low production costs and mechanical properties that render them appropriate for a number of uses, such as automotive brake disc material (Aranke et al., 2019), railroads structures (*laque1958 - Mecanismos.pdf*, s. f.), among others. The 2019 census of world casting production (*Censo 2019.pdf*, s. f.), reports that about 70% of the worldwide production of cast ferrous alloys corresponds to gray irons. On this ground, it is interesting to investigate the corrosive response of these materials in order to predict their useful life when they are exposed to the environmental conditions imposed by the marine atmosphere.

Several studies have been carried out on corrosion processes under marine atmospheres (Morcillo et al., 2013), based mainly on steels that show a bimodal behavior. A parameter denominated "ta" shows the division between two mechanisms, an aerobic and other anaerobic. These alloys, and in particular weathering steels, show the formation of a double layer of corrosion products, formed mainly by akaganeite, lepidocrocite, and goethite. The layer of goethite formed is strongly adherent and compact, which helps to protect the underlying metal from further corrosion. Goethite also has a low solubility in water, which makes it an effective barrier against the diffusion of corrosive agents (Kamimura et al., 2006; Melchers, 2008; Morcillo et al., 2013). Other studies show that grey irons subjected to marine environments, both atmospheric and immersed in seawater, form the same corrosion products reported in steels (Melchers et al., 2016). However, the corrosion mechanism has been a matter of discussion. Gray irons, unlike steels, have a microstructure composed of flakes of graphite in a matrix akin to steel. Different authors have chosen to extend the bimodal mechanism described for steels to the behavior of cast irons (Melchers et al., 2016) while others have presented a different situation considering microstructural aspects (*LaQue,1958*).

The present work, by means of an accelerated corrosion test developed and validated in weathering steels (Artigas et al., 2015), seeks to evaluate the behavior under a marine atmosphere of an austenitic gray iron of a composition based on information compiled by Melchers (Melchers, 2013a), with the purpose of generating experimental data to propose a corrosion mechanism. In order to evaluate the applicability of the accelerated corrosion test to the case of gray irons, the experimental results of this work are compared with data obtained in real-time from exposure to weathering in a marine environment (Melchers et al., 2016). For the above, the corroded thickness over time was determined and the morphology of the corrosion products was characterized.

MATERIALS AND METHODS

Two 220x225x32 [mm] gray iron billets were cast at the facilities of the Metallurgy Department of the University of Santiago de Chile, their chemical composition being determined by optical emission spectrometry (Spectro, Kleve, Germany). An initial evaluation of the cast billets' microstructural characteristics was carried out. Metallographic examinations were conducted by optical microscopy (OM) (Olympus, Tokyo, Japan) and scanning electron microscopy (SEM) after the samples had been grinded with SiC paper and polished with polycrystalline diamond suspension and then etched using Kalling's etchant according to the procedure described in the ASTM E3 standard (*ASTM E3, 2011.*); the microstructure was revealed according to the specifications of the ASTM E407 (*ASTM E407*, 2017) standard. Using comparative charts, the graphite morphology was determined according to the procedure described in the ASTM A247 standard (*ASTM A247*, 2021). Then, the billets were cut into

25x30x7 [mm] coupons, the surfaces of which were grinded using 80 to 600 sandpaper (Artigas et al., 2015). Then, they underwent an accelerated corrosion process consisting of repetitive wetting cycles. The ground samples were subjected to a salt spray wetting process based on ASTM B117 (*ASTM B117*, 2019) standard for 16 hours. Subsequently, they were allowed to rest for 50 minutes and then washed intensively for 10 minutes. After that, they were dried for 2 hours before being wetted again for another 2 hours. Then, they were left to rest for 1 hour before being subjected to another 2-hour drying phase. In this way, a cycle of 24 hours was completed, a total of forty cycles were applied to the samples. After each of the cycles 5, 10, 15, 20, 25, 30, 35, and 40, three corroded coupons were analyzed, and their mass variation was determined using one of the electrolytic pickling processes described in the ASTM G1 standard (*ASTM G1*, 2019). The loss in thickness was plotted against exposure time and the resulting curve was compared to those that by Melchers (Melchers, 2013). After corrosion cycles 10 and 20, observations were made using scanning electron microscopy to assess the characteristics of the corrosion products and the distribution of elements (carbon, nickel, and oxygen) by compositional mapping on the corroded layer.

RESULTS AND DISCUSSION

Table 1 shows that the chemical composition of the billets (GCI Billet) is, as intended, almost identical to the one reported by Melchers (Melchers, 2013a), which allowed obtaining an austenitic cast iron with type VII E4 graphite flakes (Figure 1). In the figure 1, two optical micrographs obtained at 100x and 500x of the GCI billet can be observed. The microstructure is composed of graphite, austenite, and a small amount of carbides. A SEM analysis allowed identifying the small amount of white phase observed in the micrograph as a chromium carbide, see figure 2 and table 2 for the chemical composition of the carbide and the matrix.

The corroded thickness after subjecting the GCI coupons to the accelerated corrosion process is shown in figure 3, where a bi-modal behavior, characterized by a change in the corrosion rate around cycle 20, is readily apparent.

In Figure 3, a change in slope can be observed, which is identified by the label "ta". Prior to time "ta", it is estimated that corrosion products begin to form and grow rapidly due to the supply of oxygen and water. However, upon reaching a critical value (ta), the layer of corrosion products increases, decreasing its permeability and hindering the passage of oxygen, thereby reducing the corrosion rate. With decreasing oxygen content, the corrosion process is postulated to be influenced by the presence of anaerobic bacteria (Melchers, 2007). This process, which typically takes years (Melchers, 2008), is also observed upon exposure to accelerated corrosion testing.

To compare the results obtained with those reported in the literature, information on corrosion processes in real-time of machined cast austenitic steel and austenitic gray cast irons were taken from the work of Melchers and replotted. The steel was exposed to a mid-tide environment, and the cast iron, to a coastal marine atmosphere (Melchers, 2013a). This graph, is compared to the one shown in Figure 3 with a change in scale. Figure 4 shows both graphs. The upper image figure 4a, the one obtained from the literature, and lower image figure 4b, the one obtained from the results of accelerated corrosion of this work; it is important to note that one cycle corresponds to one day. It is possible to appreciate that, even though the corrosion processes are different (mid-tide and simulated marine atmosphere), the results exposed by the

ID	%C	%Ni	%Cr	%Si	%Cu	%Mn	%P	%S	%Fe
Aust Cast Iron (GCI Billet)	2.73	17.6	2.23	3.16	0.79	0.91	0.31	0.060	Rem.
Aust Cast Iron (Melchers)[2]	2.66	17.9	2.29	3.17	0.80	0.94	0.24	0.104	Rem.

Table 1. Chemical composition of the samples.

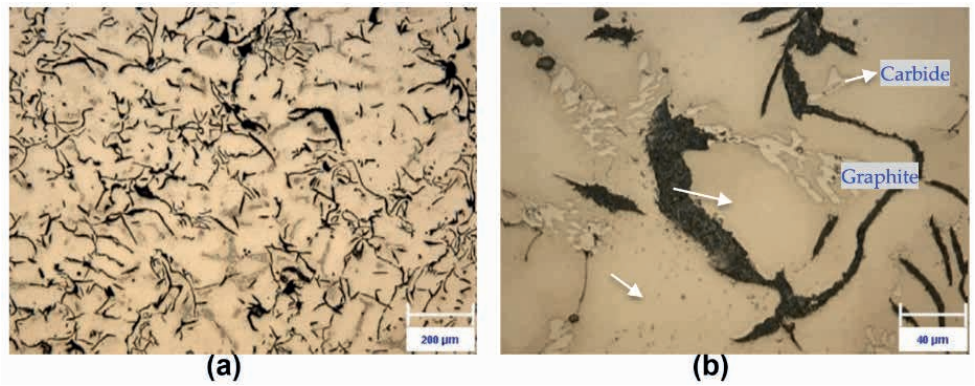

Figure 1. Optical micrograph of the GC+I billet. (a) OM at 100x (b) OM at 500x. The microstructure is composed of graphite, austenite, and a small amount of carbides.

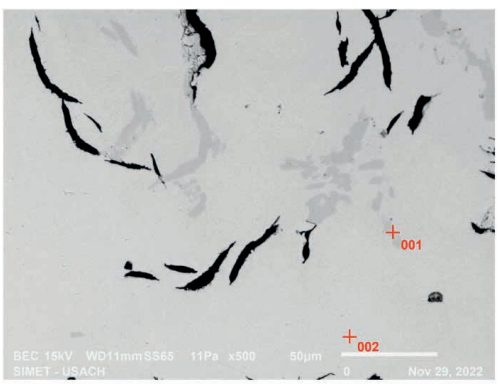

Figure 2. Scanning electron microscope image of the CGI billet.

ID	%C	%Cr	%Ni	%Fe
001	9.02	24.17	1.97	Remainder
002	5.28	1.42	19.35	Remainder

Table 2. Chemical composition obtained in scanning electron microscope by EDS.

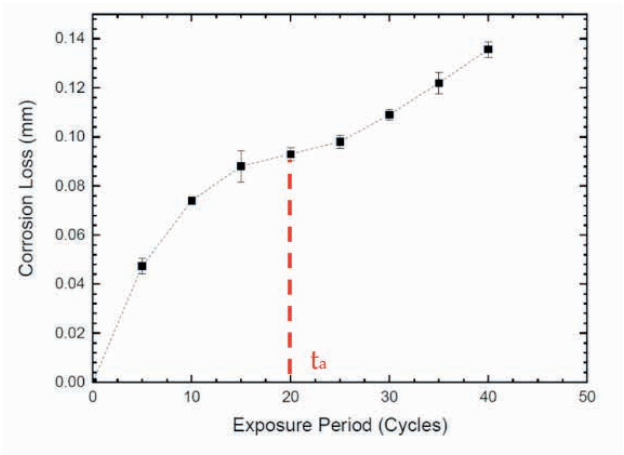

Figure 3. Graph of corroded thickness vs. time.

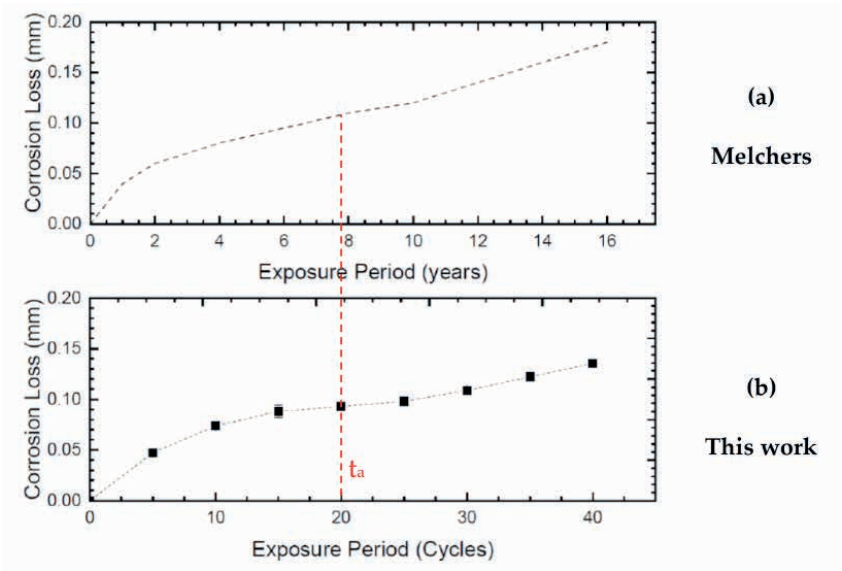

Figure 4. Comparative graphs of Corrosion Loss vs. time. a) obtained from the literature (Melchers, 2013a) b) results obtained in this work.

accelerated corrosion test present a significant similarity in scale and form. To date, it is possible to mention that corrosion processes can be homologated for up to 16 years in 40 days of testing for the alloy under study. From the above, it is possible to show that accelerated corrosion processes based on salt spray chambers could provide information on similar processes in marine corrosion.

Once the corrosion, wetting, and drying process were finished, the corrosion deposits present in the samples obtained in cycles 10 and 20 were characterized, that is, before "ta" and after this time. In figure 5, it is possible to appreciate that there is the presence of a double layer. The inner and outer layers are delimited by a dashed yellow line, that separates the presence of phases with high adhesion to the substrate from those with lower adhesion. Given the chemical composition, the inner layer is attributed to iron and nickel oxyhydroxides [17], as occurs in other steel alloys (Morcillo et al., 2013). The inner layer is in contact with the matrix of the casting, has a longer exposure time, and is associated with more stable phases, probably goethite (Inoue et al., 2008; Kamimura et al., 2006; Melchers, 2013b; Morcillo et al., 2013). The inner layer is more stable, adherent, and compact and evolves over time, increasing its thickness. For cycle 10, it has an average thickness of approximately 30 μm, while for cycle 20, it has an average thickness of approximately 50 μm. The outer layer is in contact with the environment and has a low adhesion with the inner layer. As has been described in other articles related to steel corrosion, there is an evolution of deposits (Sun et al., 2021) corresponding to the gradual transformation from lepidocrocite to goethite.

From a microstructural point of view, it is interesting to note that the presence of graphite in alloys can have a cathodic behavior, meaning it can favor or accelerate corrosion processes. The presence of graphite can promote reduction processes, such as the reduction of oxygen due to its ability to easily conduct electrons. However, the distribution of graphite flakes also plays a fundamental role in these processes. If the flakes are oriented in parallel to the surface, they act as a barrier preventing oxygen and water from coming into contact with the austenite (Fe-rich phase), thus delaying corrosion process(*LaQue,1958)*. These graphite flakes remain in the oxide layer after the corrosion process occurs, as shown in Figure 5. This, combined with the increased thickness of the corrosion products layer, further slows down corrosion processes. Therefore, the morphology and distribution of graphite flakes play multiple roles in corrosion processes. Finally, it should be noted that the detected carbides could play a similar role to that of the barrier presented by graphite; however, since carbides are not conductive, their protection is greater.

CONCLUSIONS

From the results obtained, it is possible to conclude that the tests carried out in a fog chamber, following wetting and drying processes, allow to obtain corroded thickness curves not only in the marine environment but also in the vicinity of these processes as is mid-tide. The results obtained show that the samples under study present a bi-modal behavior, such as weathering steels and others, however, the corrosion mechanisms are different. In the case of GCI, the presence of graphite can accelerate up or slow down the corrosion process depending on its distribution on the surface (*LaQue,1958*) and show a bi-modal behavior(Melchers, 2013). In addition, it is possible to mention that obtaining corrosion curves of 12 years in 40 days for this type of alloy is an advantage for the study of corrosion processes. The behavior characteristics over time are consistent with

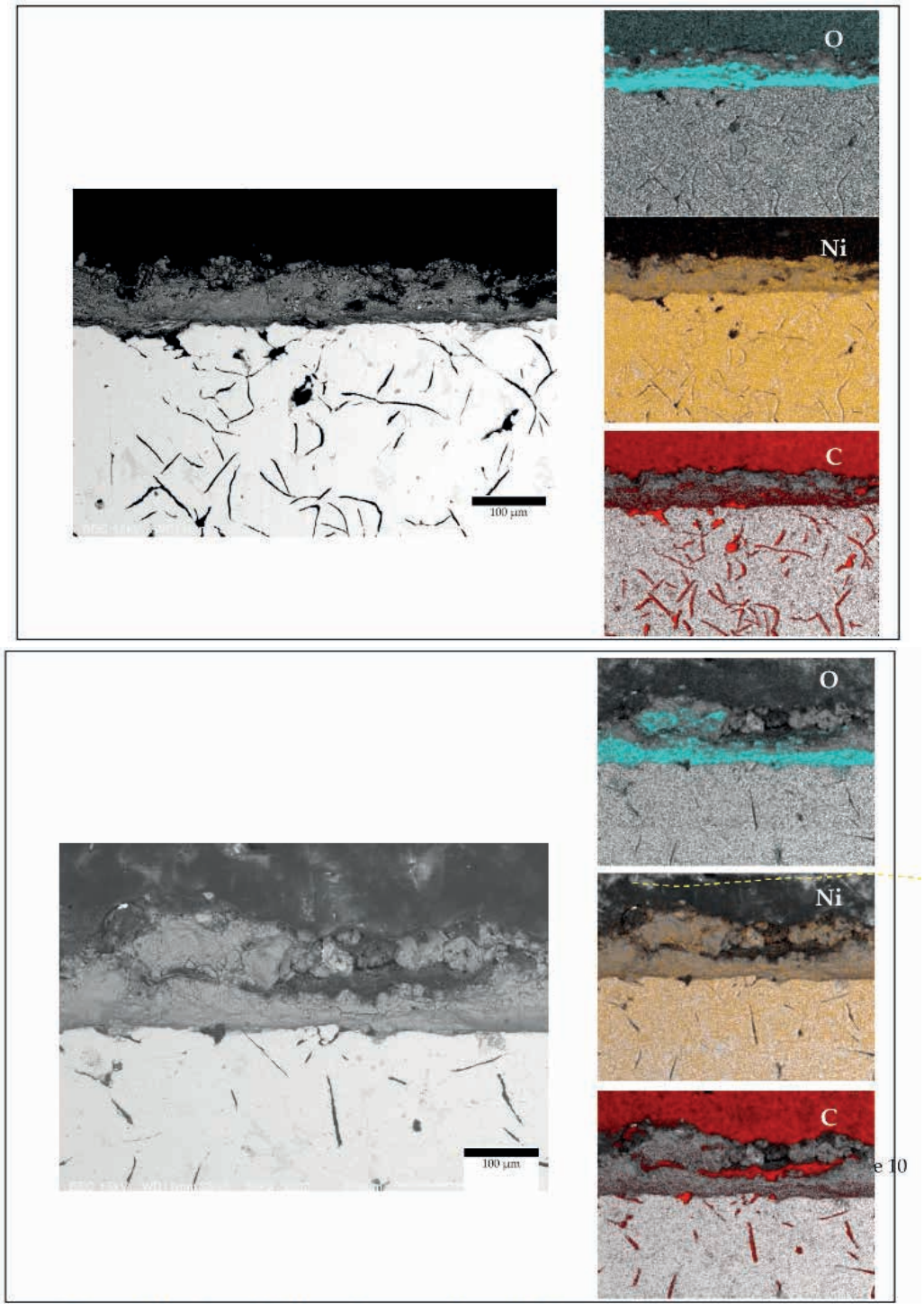

Figure 5. Mapping of Cr, N and O in cycle 10 and 20. After and before t_a.

those obtained in the field by other authors. Finally, it is confirmed that the accelerated corrosion process proposed by the research group could be used not only in steel but also in gray cast iron. The study of different graphite distributions in laminar and nodular gray iron castings and their impact on corrosion processes is proposed as future work.

DECLARATIONS

Author Contributions

H.B., A.A. and R.A. conceived the study and supervised the experimental work, H.B. writing- original draft preparation. writing-review, editing and translation A.A., R.A. L.C., A.M. O.B. and H.B. - All authors have read and agreed to the published version of this manuscript.

ACKNOWLEDGMENTS AND FUNDING

Héctor Bruna wishes to express his sincere gratitude to the "Agencia Nacional de Investigación y Desarrollo (ANID)" particularly to the national doctoral scholarship that allows the training of advanced human capital in Chile.

Rodrigo Allende wishes to express his sincere gratitude to the "Dirección de Investigación Científica y Tecnológica (DICYT)" of the Universidad de Santiago de Chile (USACH) for funding the 052214AS project, which allowed for significant progress in our research.

Alberto Monsalve wishes to express his gratitute to "Programa de Integridad Estructural"

All authors who wish to express their gratitude to DICYT-USACH, that allows the development of this type of work.

REFERENCES

AMPP (Association for Materials Protection and Performance). (2021). 2021 Impact Canada Study: Corrosion. Houston, Texas: NACE International.

Aranke, O., Algenaid, W., Awe, S., & Joshi, S. (2019). Coatings for Automotive Gray Cast Iron Brake Discs: A Review. Coatings, 9(9), 552. https://doi.org/10.3390/coatings9090552

Artigas, A., Monsalve, A., Sipos, K., Bustos, O., Mena, J., Seco, R., & Garza-Montes-de-Oca, N. (2015). Development of accelerated wet–dry cycle corrosion test in marine environment for weathering steels. Corrosion Engineering, Science and Technology, 50(8), 628-632. https://doi.org/10.1179/1743278215Y.0000000007

ASTM International. (2011). ASTM E3-11, Standard Guide for Preparation of Metallographic Specimens. ASTM International.

ASTM International. (2017). ASTM E407-17 Standard Test Method for Microetching Metals and Alloys. ASTM International.

ASTM International. (2021). ASTM A247-20: Standard test method for evaluating the microstructure of graphite in iron castings. ASTM International.

ASTM International. (2019). ASTM B117/B117M-19 - Standard Practice for Operating Salt Spray (Fog) Apparatus. ASTM International.

ASTM International. (2019). ASTM G1-03(2019): Standard Practice for Preparing, Cleaning, and Evaluating Corrosion Test Specimens. ASTM International.

Modern Casting. (2019). Census of World Casting Production. Obtained from < https://www.thewfo.com/contentfiles/downloads/51.pdf >

Harsimran, S., Santosh, K., & Rakesh, K. (2021). Overview of corrosion and its control. A critical review. Proceedings on Engineering Sciences, 3(1), 13-24. https://doi.org/10.24874/PES03.01.002

Inoue, K., Shinoda, K., Suzuki, S., & Waseda, Y. (2008). Characteristic Behavior of Nickel Ions during Transformation of Green Rust to Ferric Oxyhydroxides in Aqueous Solution. MATERIALS TRANSACTIONS, 49(3), 466-470. https://doi.org/10.2320/matertrans.MBW200710

Kamimura, T., Hara, S., Miyuki, H., Yamashita, M., & Uchida, H. (2006). Composition and protective ability of rust layer formed on weathering steel exposed to various environments. Corrosion Science, 48(9), 2799-2812. https://doi.org/10.1016/j.corsci.2005.10.004

LaQue, F. L. (1989). The corrosion resistance of ductile iron. Materials Performance, 28(3), 51-56.

Melchers, R. E. (2007). Transition from Marine Immersion to Coastal Atmospheric Corrosion for Structural Steels. CORROSION, 63(6), 500-514. https://doi.org/10.5006/1.3278401

Melchers, R. E. (2008). A new interpretation of the corrosion loss processes for weathering steels in marine atmospheres. Corrosion Science, 50(12), 3446-3454. https://doi.org/10.1016/j.corsci.2008.09.003

Melchers, R. E. (2013a). Long-term corrosion of cast irons and steel in marine and atmospheric environments. Corrosion Science, 68, 186-194. https://doi.org/10.1016/j.corsci.2012.11.014

Melchers, R. E. (2013b). Microbiological and abiotic processes in modelling longer-term marine corrosion of steel. Bioelectrochemistry (Amsterdam, Netherlands), 97. https://doi.org/10.1016/j.bioelechem.2013.07.002

Melchers, R. E., Herron, C., & Emslie, R. (2016). Long term marine corrosion of cast iron bridge piers. Corrosion Engineering, Science and Technology, 51(4), 248-255. https://doi.org/10.1179/1743278215Y.0000000049

Morcillo, M., Chico, B., Díaz, I., Cano, H., & de la Fuente, D. (2013). Atmospheric corrosion data of weathering steels. A review. Corrosion Science, 77, 6-24. https://doi.org/10.1016/j.corsci.2013.08.021

Schmitt, G. (s. f.). Global Needs for Knowledge Dissemination, Research, and Development in Materials Deterioration and Corrosion Control. 48.

Sun, M., Du, C., Liu, Z., Liu, C., Li, X., & Wu, Y. (2021). Fundamental understanding on the effect of Cr on corrosion resistance of weathering steel in simulated tropical marine atmosphere. Corrosion Science, 186, 109427. https://doi.org/10.1016/j.corsci.2021.109427